Xylem Embolism Spreads by Single-Conduit Events in Three Dry Forest Angiosperm Stems[1][OPEN]

Kate M. Johnson,[a] Craig Brodersen,[b] Madeline R. Carins-Murphy,[a] Brendan Choat,[c] and Timothy J. Brodribb[a,2,3]

[a]Discipline of Biological Sciences, School of Natural Sciences, University of Tasmania, Hobart, Tasmania 7001, Australia
[b]School of Forestry and Environmental Studies, Yale University, New Haven, Connecticut 06511
[c]Hawkesbury Institute for the Environment, Western Sydney University, Penrith, New South Wales 2750, Australia

ORCID IDs: 0000-0002-3039-6339 (K.M.J.); 0000-0002-0924-2570 (C.B.); 0000-0003-4370-9485 (M.R.C.-M.); 0000-0002-9105-640X (B.C.); 0000-0002-4964-6107 (T.J.B.).

Xylem cavitation resulting in air embolism is a major cause of plant death during drought, yet the spread of embolism throughout the plant water transport system is poorly understood. Our study used optical visualization and x-ray microcomputed tomography imaging to capture the spread of emboli in stems of three drought-resistant angiosperm trees: drooping she-oak (*Allocasuarina verticillata*), black wattle (*Acacia mearnsii*), and blue gum (*Eucalyptus globulus*). These species have similar degrees of xylem network connectivity (vessel grouping) with largely solitary vessels. The high temporal resolution of the optical vulnerability technique revealed that in current year branches, >80% of the cavitation events were discrete, temporally separated events in single vessels. This suggests that in xylem networks with low connectivity, embolism spread between conduits leading to multiple conduit cavitation events is uncommon. *A. mearnsii* showed both the highest number of multivessel cavitation events and the highest degree of vessel connectivity, suggesting a link between vessel arrangement and embolism spread. Knowledge of embolism spread will help us to uncover the links between xylem anatomy, arrangement, and the path of water flow in the xylem in diverse species to ultimately understand the drivers of cavitation and plant vulnerability to drought.

Increasingly severe, prolonged, and frequent droughts are leading to large-scale forest dieback across the globe (Pachauri and Meyer, 2014; Sheil, 2014; Allen et al., 2015; Millar and Stephenson, 2015; Young et al., 2017). Complete or partial blockage of the plant vascular system due to cavitation and subsequent desiccation of meristematic tissues is the principle cause of plant death during drought events (Choat et al., 2012; Anderegg et al., 2016; Brodribb et al., 2020). To understand, accurately model, and ultimately mitigate these patterns of tree mortality we must uncover how vascular failure spreads though woody plants during drought stress.

Plants require an uninterrupted supply of water for normal function, photosynthesis, growth and reproduction. Water is transported through plants under negative pressure (otherwise referred to as "tension") via a network of interconnected pipes called xylem conduits, as described by the cohesion-tension theory (Dixon, 1914; Dixon and Joly, 1895; Tyree and Zimmermann, 2002). In drought conditions, drying soil reduces water availability to the roots causing xylem tension to increase. When this tension reaches a critical threshold, air can aspirate across membranes that separate adjacent xylem conduits, nucleating the formation of air bubbles or embolisms in a process called cavitation by air seeding (Lewis, 1988; Tyree and Sperry, 1988). Air emboli resulting from cavitation block the flow of water through the plant and if drying continues, increasing xylem tension leads to more cavitation, potentially initiating a feedback process that leads to plant death in drought conditions (Tyree and Sperry, 1988; Brodribb and Cochard 2009; Choat et al., 2012).

Traditional flow-based methods, which require excised stem segments, have been used to determine plant vulnerability to drought by identifying water stress

[1]This work was supported by the Australian Synchrotron (project no. 14069 to B.C.), the Department of Industry, Innovation, Science, Research and Tertiary Education of the Australian Government Research (Training Program Scholarship to K.M.J.), and the Australian Research Council (grant no. DP190101552).

[2]Author for contact: timothy.brodribb@utas.edu.au.
[3]Senior author.

The author responsible for distribution of materials integral to the findings presented in this article in accordance with the policy described in the Instructions for Authors (www.plantphysiol.org) is: Timothy J. Brodribb (timothy.brodribb@utas.edu.au).

T.J.B. conceived and designed the original concept of the experiment; K.M.J., M.C.M., and T.J.B. designed and performed the experiments; K.M.J. analyzed the data and wrote the manuscript with contributions from all authors; C.B. provided technical assistance with data analysis; and B.C. facilitated acquisition of scanning time at the Australian Synchrotron.

[OPEN]Articles can be viewed without a subscription.
www.plantphysiol.org/cgi/doi/10.1104/pp.20.00464

thresholds beyond which cavitation occurs in the xylem. However, these methods provide little information about the timing and spatial spread of cavitation-induced damage through the vascular system in intact plants. Newly developed imaging methods enable direct visualization of cavitation events in situ, providing new tools for understanding how xylem network organization influences cavitation spread and losses in conductivity. Techniques include nuclear magnetic resonance imaging, high-resolution x-ray microcomputed tomography (microCT), and the optical vulnerability technique (OVT). This presents the opportunity to examine links between the anatomy and arrangement of the plant water transport system, embolism spread, and vulnerability to drought-induced damage and death.

Vulnerability to xylem cavitation is highly variable among species (Maherali et al., 2004; Choat et al., 2012; Larter et al., 2017) and is correlated with species distribution and their susceptibility to damage during drought (Pittermann et al., 2012; Skelton et al., 2015). Thus, there is a strong imperative to understand how xylem characteristics influence the xylem vulnerability of a species or individual. Anatomical and network properties of the xylem conduit network have been used to create theoretical models to describe how water moves through plants (Loepfe et al., 2007; Lee et al., 2013; Mrad et al., 2018). The number and spatial distribution of interconduit connections and the properties of pit membranes within them are likely to be some of the most important traits influencing embolism spread through the vessel network (Choat et al., 2008). The distribution and anatomy of the pits between conduits is hypothesized to determine the propensity for air to break into the water column (Sperry et al., 1996) and is thought to be closely linked to the spread of embolism between conduits (Wheeler et al., 2005; Choat et al., 2008; Schenk et al., 2008). Comparing the arrangement of xylem in the network with the pattern and progression of embolism will allow us to gain insight into how xylem connectivity influences embolism spread.

While it is likely that a combination of anatomical traits contribute to species vulnerability, one critical aspect is related to the distribution of the highly conductive, specialized conduits characteristic of angiosperms: the vessels. Vessel connectivity is critical as intervessel connections provide potential pathways for the movement of air embolisms in the xylem network. Xylem grouping (where a group is defined as two or more vessels sharing a wall; Carlquist, 2001) has been shown to be correlated with the patterns of embolism spread (Hacke and Sperry 2001; Schenk et al., 2008; Choat et al., 2016; Medeiros et al., 2019). It has been suggested that vessel grouping and clustering of the xylem into discrete sectors may create redundancy in the hydraulic pathway and reduce embolism spread (Carlquist 1966; Carlquist 1984; Schenk et al., 2008; Zhao 2016). In contrast, it has also been proposed that vessel grouping and clustering may increase the chance of emboli spreading between adjoined or neighboring vessels (Loepfe et al., 2007). Schenk et al. (2008) found that modular, segmented basal stems (composed of many individual stems grouped together) were associated with shrubs living in arid environments, while shrubs in more humid environments had singular basal stems with more hydraulically integrated vessel networks, suggesting that segmentation may increase redundancy in the hydraulic pathway at multiple scales. Although xylem anatomy and loss of xylem function have been explored separately, the relationship between spatial arrangement and xylem vulnerability has been theorized (Loepfe et al., 2007) but not tested. As connectivity in the vessel network influences embolism spread, it is likely that different degrees of vessel grouping are associated with different degrees of vulnerability, making xylem connectivity a possible driver of drought resistance and species distribution.

Direct observation techniques like microCT and the OVT can be used to investigate embolism spread by determining the frequency of cavitation events involving more than one individual vessel (i.e. multiple events) and those in which one individual vessel cavitates in a single image frame (single cavitation events).

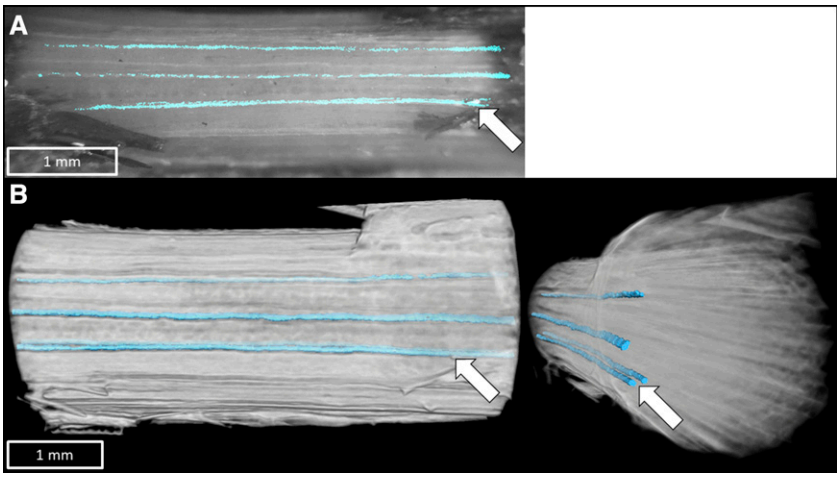

Figure 1. Cavitation visually resolved using OVT matches cavitation resolved with microCT. Clear spatial correspondence can be seen between the newly cavitated vessels (blue) identified in the same stem region of *A. verticillata* using the two methods, OVT (A) and microCT (B). Both methods identified a cumulative total of four vessels that cavitated over ~8 h of stem dehydration. The cross-sectional view from the microCT (right) reveals that two of the four cavitated vessels were closely aligned in the stem (white arrows indicate this vessel pair in all images), but despite this they could still be resolved as a vessel pair using the OVT.

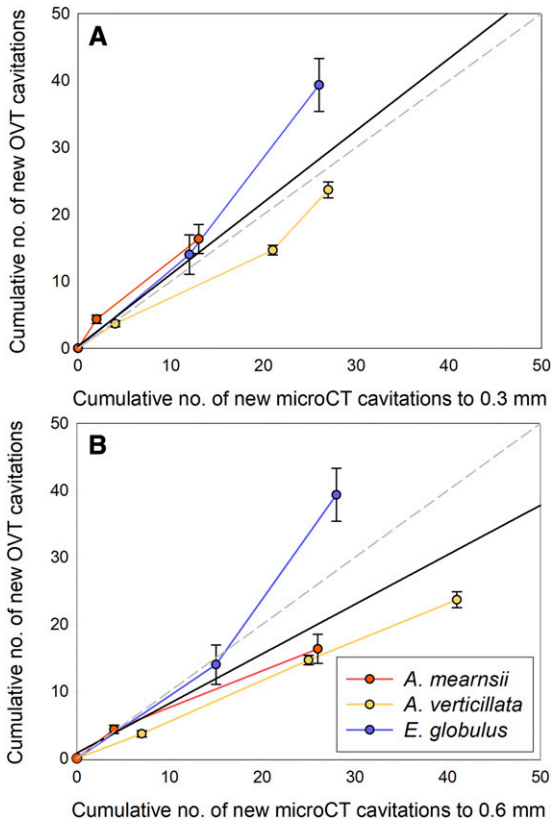

Figure 2. Cumulative cavitations resolved with both microCT and the OVT at depths of 0.3 and 0.6 mm into stems. Cumulative new microCT cavitation events are shown versus cumulative new OVT cavitation events at 0.3 mm (A) and 0.6 mm (B) in the OVT-visualized regions for *A. mearnsii* (red), *A. verticillata* (gold), and *E. globulus* (blue). Data points generated using the OVT are the average of three slices of the OVT images (see "Materials and Methods") and the error bars (SE) show the variation between cavitation counts for these three slices. Solid black lines show the regressions through all data points and the gray dashed lines show the 1:1 relationship.

Studies in leaf veins have shown that multiple synchronous cavitation events commonly occur among vein orders in the leaves of ferns (Brodribb et al., 2016a), grasses (Johnson et al., 2018), and angiosperms (Brodribb et al., 2016a, 2016b). Observation of cavitation formation in the stems of grapevine (*Vitis vinifera*), walnut (*Juglans* spp.), and redwood using microCT also revealed instances where discrete sectors of xylem cavitate together (Brodersen et al., 2013; Choat et al., 2015; Knipfer et al., 2015). Combining these techniques allows us to resolve events with both high spatial resolution, using microCT (Cochard et al., 2015; Choat et al., 2016) and high temporal resolution with the OVT. While the short time interval between images captured using the OVT (2 min) allows us to visualize embolism spread between conduits at a high temporal scale, it remains to be seen whether the resolution of the two-dimensional spatial information from the OVT corresponds to the high-resolution, three-dimensional (3D) spatial information provided by microCT. Here we make this assessment and combine these techniques to construct a high-resolution temporal map of embolism spread in stems.

In this study, we monitored embolism spread concurrently using the OVT and microCT with a focus on vessel networks as opposed to tracheid networks. This enabled us to (1) assess the reliability of the spatial information provided by the OVT, and (2) use the temporally and spatially resolved OVT cavitation data to assess the radial spread of cavitation in woody stems. We chose to test this using three co-occurring woody angiosperm trees, *Acacia mearnsii*, *Allocasuarina verticillata*, and *Eucalyptus globulus*. All species are drought resistant long-vesseled angiosperms with predominantly solitary, spatially separated xylem vessels, which provided an opportunity to assess the spread of embolism in species with similar degrees of xylem network connectivity. Typically, our understanding of embolism spread is based on the assumption that cavitation events will only propagate between vessels that are radially or axially connected and the idea that vessels differ in their vulnerability to air seeding (Christman et al., 2012; Venturas et al., 2016; Wason et al., 2018).

It is possible that the pattern of embolism spread is linked to the connectivity of the xylem conduit network. If the chance of vessel-vessel propagation of embolism is proportional to the number of pit membranes that must be crossed between them (Choat et al., 2008), higher conduit-network connectivity would mean a higher number of cavitation events involving multiple conduits. In stems with minimal vessel connections and vessel clustering, we predicted that the progression of cavitation would be gradual, dominated by single events, in contrast to that observed in more interconnected conduit networks such as angiosperm leaves (Brodribb et al., 2016a, 2016b).

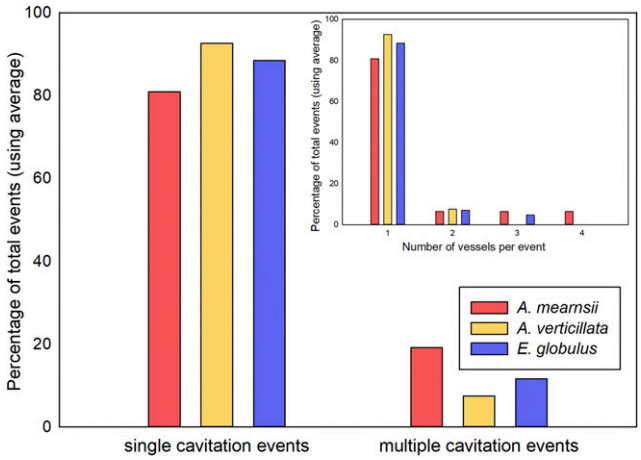

Figure 3. Single- and multiple-vessel OVT cavitation events expressed as a percentage of total events. Single and multiple stem cavitation events observed using the OVT in *A. mearnsii* (red), *A. verticillata* (gold), and *E. globulus* (blue), expressed as a percentage of the total number of cavitation events. The inset shows these cavitation events broken down into the number of simultaneous events per image (1–4), expressed as a percentage of the total events.

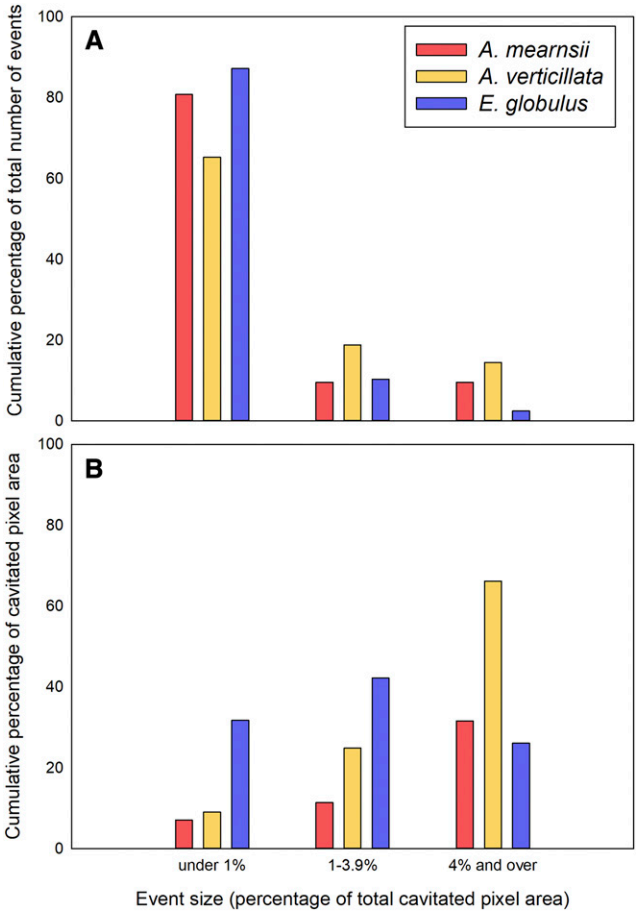

Figure 4. OVT cavitations sorted by size and expressed as both a percentage of the total number of events and a percentage of the total cavitated pixel area. The relative cumulative contribution of OVT cavitation events of three size classes (<1%, between 1% and 3.9%, and >4% of the total pixel area of cavitated vessels) to the total number of events (A) and the total pixel area of cavitated vessels (B) in the stems of *A. mearnsii* (red), *A. verticillata* (gold), and *E. globulus* (blue).

RESULTS

Cross-Validation of OVT and MicroCT for Detecting Cavitation Events

In all three species we were able to identify identical cavitation events in both the OVT and microCT images (Fig. 1). Changes to the intensity of light reflected from the xylem in the OVT were found to be spatially associated with discrete embolisms identified in microCT images (Fig. 1).

Maximum Tissue Depth for Cavitation Detection Using the OVT

Using microCT, the number of new cavitation events detected between time points in stem tissue from the xylem surface to a depth of 0.3 mm into the stem in *A. verticillata* and *A. mearnsii* closely corresponded with those detected using the OVT (Fig. 2). In *E. globulus*, however, ~33% more events were recorded with the OVT than with microCT in this region of the stem (i.e. from the xylem surface to 0.3 mm deep; Fig. 2). When a larger stem region (from the xylem surface to a depth of 0.6 mm into the stem) was examined, the extent of this agreement became more variable among species (Fig. 2). During the early stages of cavitation, there was close agreement between the number of new cavitation events detected in this region of the stem by both methods in all species. However, at later stages of cavitation, the OVT detected fewer events than microCT. Specifically, the OVT detected ~60% of the events detected by microCT in *A. verticillata* and ~70% in *A. mearnsii*, whereas in *E. globulus* the OVT detected ~33% more cavitation events than microCT (Fig. 2). Furthermore, in all three species bark removal did not alter the progression of cavitation. Thus, embolism spread did not vary between the region of xylem below the removed bark and the region of xylem below the intact bark (Supplemental Figs. S1 and S2). A linear regression with a slope of 0.86 (with a slope of 1 falling within the 95% confidence interval) described the relationship between the number of cavitation events detected in the stem from the xylem surface to a depth of 0.3 mm below removed bark and below the intact bark (expressed as a percentage of total events) at two time points within one stem of each of the three species (Supplemental Fig. S2).

Temporal Pattern of Cavitation Events

In each of the three experimental species, more than 80% of the total number of cavitations were discrete (comprised single vessels), and temporally isolated, where there was only a single cavitation event within each 2-min interval (Fig. 3). The remaining events were multiple events, where more than one cavitation event occurred during the 2-min interval. Multiple-event observations occurred most frequently in *A. mearnsii*, representing 19% of the total number of events, followed by *E. globulus* (12%) and *A. verticillata* (8%; Fig. 3). In *A. verticillata*, multiple events were always paired (two vessels cavitated in a single frame), while both paired events and events with three cavitated vessels were observed in *E. globulus* (Fig. 3). Paired events, along with events where three or four vessels cavitated, were observed in *A. mearnsii* (Fig. 3).

Events that individually constituted <1% of the total cavitated pixel area in OVT images made up ~60% of the total number of events in *A. verticillata* and ~80% of events in both *A. mearnsii* and *E. globulus*. Thus, cavitation events that made up <1% of the total cavitated pixel area were more common than larger events in all species. However, these events collectively made up <10% of the total cavitated pixel area in *A. verticillata* and *A. mearnsii* and approximately one-third of the cavitated pixel area in *Eucalyptus* (31%; Fig. 4). Very

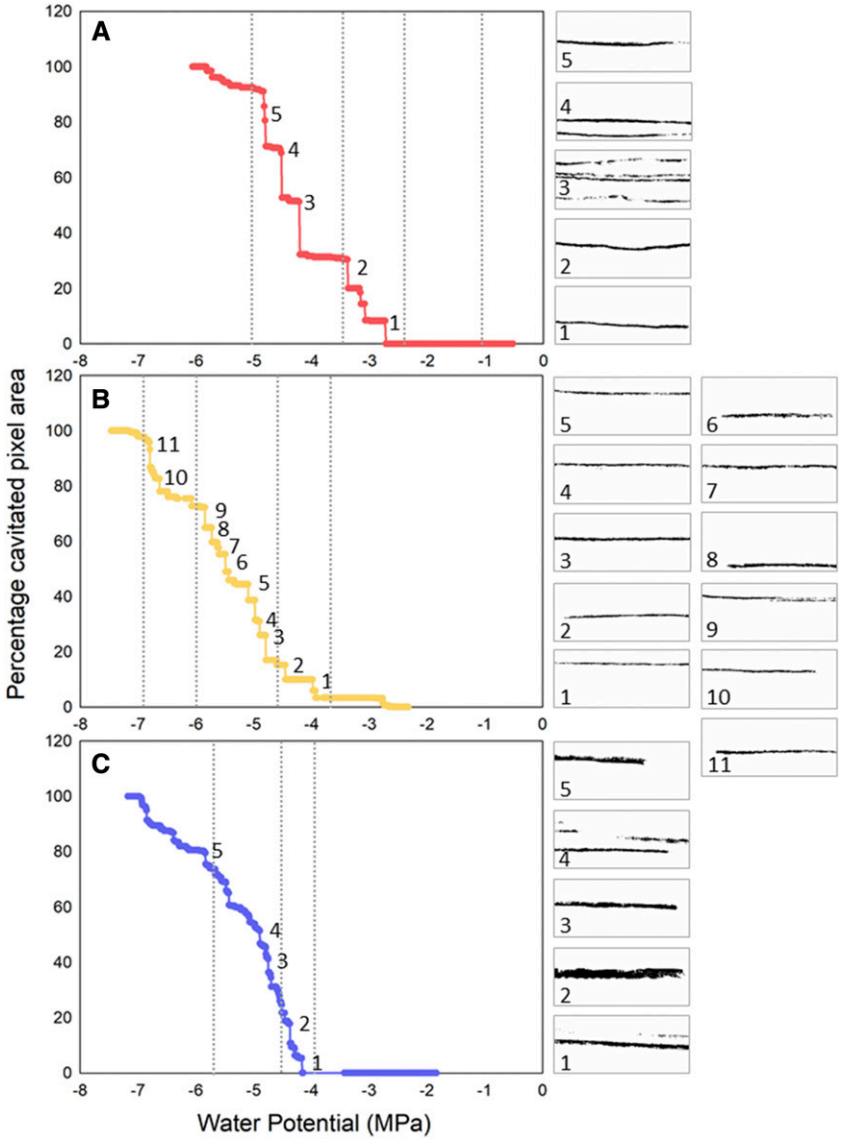

Figure 5. OVT cavitation events as a percentage of the total cavitated area against stem water potential, with the events that constitute noticeable jumps in percentage cavitation pictured. Stem water potential is shown versus OVT stem cavitation events expressed as a percentage of the total cavitated area in *A. mearnsii* (red; A), *A. verticillata* (gold; B), and *E. globulus* (blue; C). In order to provide a visual reference for the events, which constitute noticeable jumps in percentage of cavitation, large cavitations (>4% of the total cavitated area) are numbered and pictured to the right of each plot. These pictures depict newly cavitated vessels and are the result of image differences and thresholding of OVT images. Smaller cavitations make up the remainder of the cavitated area, with ~25 additional events in *A. mearnsii*, 30 in *A. verticillata*, and 50 in *E. globulus*. These plots depict all recorded OVT events, rather than average cavitation across three slices of the OVT images, to provide a complete visual representation of the progression of OVT events. MicroCT scans are represented by gray dotted lines. Note that this figure depicts the cavitation events captured using the OVT but does not show 100% stem cavitation, because the final microCT "cut" scans (not depicted here) were conducted before 100% stem cavitation was reached.

large individual cavitation events comprising >4% of the total cavitated area were few in number in all species (2% to 15% of events), but they accounted for approximately one-third of the total cavitated pixel area in *A. mearnsii* and *E. globulus* (31.57% and 26%, respectively) and approximately double this in *A. verticillata* (66.15%; Fig. 4). Of the larger events (>4% of the total cavitated area) in *A. mearnsii* and *E. globulus*, approximately half of events were singular and the other half multiple (Fig. 5). Contrastingly, in *A. verticillata*, only one out of 16 large events (event 9) was a multiple event (Fig. 5).

Vessel Size Distribution from Light Microscopy

While maximum vessel size in the stems of all species was 60 to 65 μm, *E. globulus* had more small vessels, within the 10 to 20 μm range (29.7%), compared to *A. verticillata* (15%) and *A. mearnsii* (0%; Supplemental Fig. S3).

Vessel Grouping from Light Microscopy

Two of the experimental species, *A. verticillata* and *E. globulus*, had vessel grouping indices (V_G) of ~1 within the stem region visualized using the OVT (1.02 and 1.04, respectively) whereas *A. mearnsii* had a V_G of 1.13. While the total number of vessels in the stem region visualized using the OVT from the xylem surface to a depth of 0.3 mm was consistent across species (between 70 and 80 vessels) *A. mearnsii* had more paired vessels (6 pairs, 12 vessels) than *A. verticillata* and *E. globulus* (two pairs and one pair, respectively; Fig. 6). The percentage of solitary and grouped vessels resolved using light microscopy corresponded to the percentage of single and multiple cavitation events shown in Figure 3.

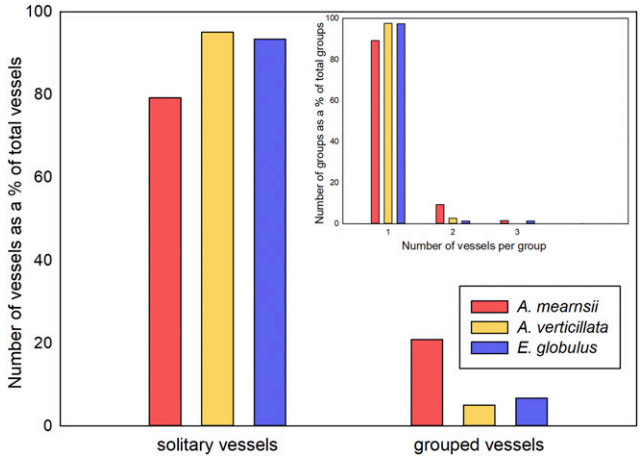

Figure 6. Number of solitary and grouped vessels as a percentage of the total number of vessels. The number of solitary and grouped vessels resolved using light microscopy from transverse sections of the stem region visualized during OVT measurements from the xylem surface to a depth of 0.3 mm in *A. mearnsii* (red), *A. verticillata* (gold), and *E. globulus* (blue) is expressed as a percentage of the total number of vessels. The inset shows the vessels in the main plot divided according to the number of individual vessels per group and expressed as a percentage of the total number of vessel groups.

DISCUSSION

In this study, we found that xylem cavitation during water stress mostly occurred as discrete, single-vessel events in the stems of three long-vesseled angiosperm trees (*A. mearnsii*, *E. globulus*, and *A. verticillata*). This is in contrast to the leaves of woody species, which are characterized by cavitation events involving multiple conduits and vein orders (Brodribb et al., 2016b). The rarity of multivessel cavitation events in our stem samples suggests that the spread of bubbles between neighboring vessels is minimal, likely due to low connectivity of the vessel networks.

In all three species, >80% of cavitation events involved only one vessel, indicating that multiple events where air spreads rapidly between connected vessels are uncommon in the stems of these species. This is contrary to observations in leaves, including those of *E. globulus*, in which cavitation events often involve multiple vein orders (Supplemental Fig. S4; Brodribb et al., 2016a, 2016b; Johnson et al., 2018). The venation networks of angiosperm leaves are highly interconnected with densely packed vessels in a reticulate network terminating in imperforate tracheary elements (Carlquist 1986; Chatelet et al., 2006). In contrast, the vessels in stems are often radially separated by other cells, particularly in the species examined here, resulting in a less connected vessel network. While single events were predicted to be common in these stems, the very low incidence of multiple cavitation events observed was unexpected. This suggests that vessel-vessel air spread may be rare in xylem networks with largely solitary vessels. The high frequency of single, discrete xylem cavitations in stems found in this study and the previously observed high proportion of multiple cavitation events in leaves suggest that the degree of xylem connectivity may explain the differences in embolism spread within these organs.

The predominace of single cavitation events in the stems observed here contrasts with data from microCT scans of other woody species (tracheid-bearing Californian redwood and vessel-bearing grapevine). In both species, cavitation appears to occur largely in "sectors," where multiple xylem vessels cavitate together (Brodersen et al., 2013; Choat et al., 2015; Knipfer et al., 2015). Although it is harder to confirm the synchrony of cavitation events in microCT systems, where scan times are often >20 min, the results from these other species also support our hypothesis of embolism spread. Both conifers and grapevine have been shown to have highly grouped xylem networks, with highly interconnected tracheid matrices present in conifer stems and clustered vessels found in grapevine (Brodersen et al., 2013; Choat et al., 2015, 2016). By contrast, vessel to vessel connections are rare in walnut stems, and cavitation events in this species are more separated in space (Knipfer et al., 2015). This is similar to the pattern observed here in *A. verticillata* and *E. globulus*. Both had vessel grouping scores very close to

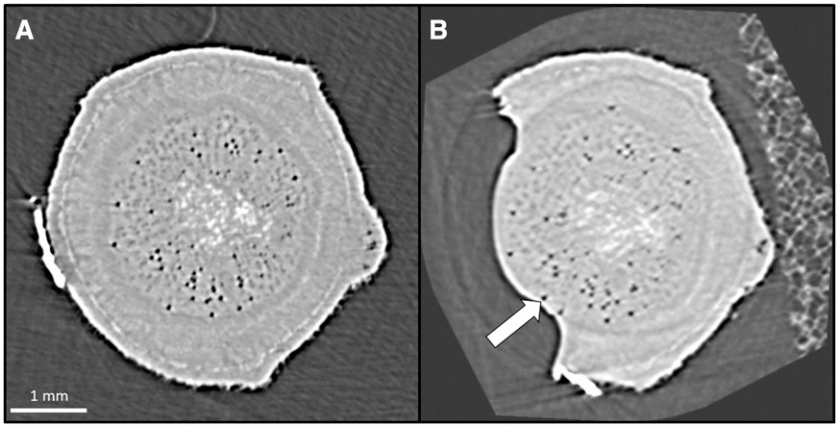

Figure 7. MicroCT scans of a stem before and after preparation for the OVT. MicroCT scans show an *A. mearnsii* stem before (A) and after (B) bark was removed from the left side of the stem and the OVT device attached. The single cavitated vessel, which may have been induced by sample preparation, is indicated by a white arrow.

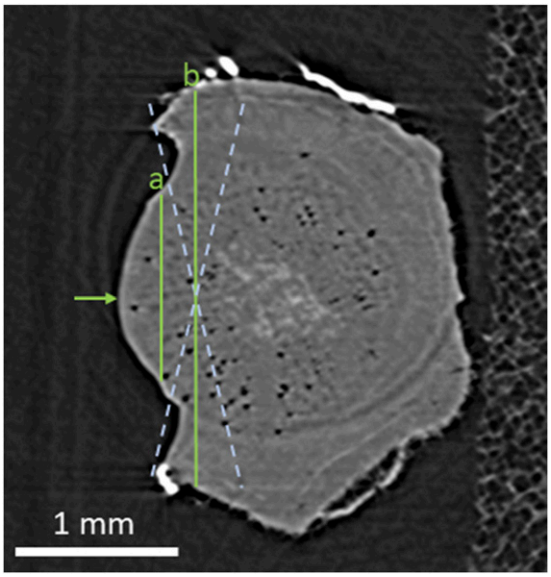

Figure 8. MicoCT scan of a stem showing the depths to which embolism was counted. A representative transverse microCT image of an *A. mearnsii* stem was used to count the number of cavitated vessels within the whole stem area at two depths indicated by green lines, 0.3 mm (a) and 0.6 mm (b) into the stem. These depths were measured from the middle of the area where bark was removed to expose the xylem (green arrow), which was deemed to be an average of all possible orientations of the stem in OVT images. Two possible orientations are indicated by light blue dashed lines. The material to the right of the stem is the foam upon which the stem was mounted in the MiCAM.

1, indicating almost completely solitary vessels, and single-vessel cavitation events were more frequent in both these species than in *A. mearnsii*.

Of the three experimental species, *A. mearnsii* exhibited multiple events most frequently. Vessel grouping, and thus connectivity, was also highest in *A. mearnsii*. This suggests that differences in embolism spread between organs, and also differences in embolism spread between species with varying levels of vessel connectivity, may be explained by increased vessel network connectivity leading to a higher chance of embolism spread between vessels (Choat et al., 2008). Here we assume that multiple events indicate connected vessels, yet it is also possible that two unconnected vessels may both cavitate within the 2-min image interval. However, the more frequent grouping of vessels in *A. mearnsii* supports the notion that greater hydraulic connectivity results in more events involving multiple vessels.

While vessel grouping was slightly higher in *A. mearnsii* compared to *A. verticillata* and *E. globulus*, in the broader context of xylem anatomies, all three stems have predominantly solitary vessels. The degree of vessel grouping was calculated at the site of OVT and microCT imaging for each branch, enabling direct comparison between xylem connectivity and embolism spread in the samples. This allows us to have confidence in the observation that *A. mearnsii* had both higher vessel grouping and higher incidence of multiple cavitation events, suggesting that variation in stem embolism spread between species may be driven by subtle differences in xylem connectivity. However, it is important to note that the variation in vessel grouping and embolism spread observed here may be due to individual differences in the samples rather than broader differences between species. The lack of within-species replication in this study is due to limited access to microCT scanning facilities and the intensive nature of monitoring embolism by both microCT and OVT concurrently. However, due to the similarity in vessel connectivity between the three samples, our overarching observation that cavitation was dominated by single-conduit events in all three stems provides convincing evidence that this pattern of embolism is characteristic of stems with low vessel connectivity. To determine whether the pattern of embolism spread is intrinsically linked to xylem network arrangement, further quantification of embolism spread and vessel network connectivity across species with diverse xylem anatomies is required.

Individual cavitation events were identified using both the OVT and microCT. Thus, an event observed using the OVT was spatially and temporally matched to its corresponding record in microCT scans, providing an important cross validation of these techniques as reliable tools for observing the deterioration of water transport capacity in the xylem. Furthermore, no evidence was found to support qualitative observations of artefacts associated with bark removal (visible disturbance to the xylem caused by sample preparation was negligible), and no difference was observed in the appearance of the stem between the barked and de-barked regions (Venturas et al., 2019). We speculate that qualitative obervations by Venturas et al. (2019) may result from their use of oil-based products on the stem surface

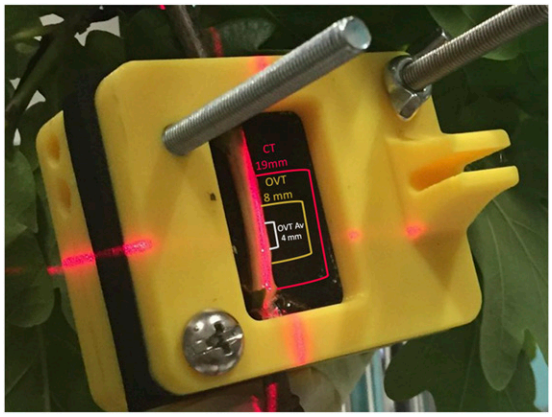

Figure 9. Image of the set-up for microCT scanning of stems. A current-year stem secured in a MiCAM (yellow) was positioned in the beamline prior to microCT scanning, as indicated by the red crosshairs. The red bracket denotes the microCT scan area, the yellow bracket shows the OVT field of view, and the white bracket indicates the portion of the OVT data that was analyzed for cavitations.

rather than hydrogel as recommended by previous studies. The congruence in observations of cavitation events between the two techniques confirms that the changes in light intensity recorded as "events" in the OVT are associated with xylem cavitation.

The OVT reliably resolved cavitation to a depth of 0.3 mm into the stems of two of the three experimental species (*A. mearnsii* and *A. verticillata*). By comparing emboli detected using the OVT and microCT, embolism at this depth was found to be representative of embolism across the entire stem cross section when small branches (2–3 mm in diameter) were studied. This was also supported by similarity in the relative frequency of single and multiple events observed with the OVT and the relative frequency of solitary and grouped vessels resolved using light microscopy from transverse sections of the stem region visualized using the OVT from the xylem surface to a depth of 0.3 mm. We found that a large proportion of early cavitation events could be detected with the OVT to a depth of 0.6 mm into the stem, but cavitation detection declined in *A. mearnsii* and *A. verticillata* at later stages of cavitation. This indicates that over time, as more emboli accumulate, those deeper in the stem may become harder to resolve. This may impact indices of stem xylem vulnerability to cavitation, for example, the "P50," which is the water potential at which 50% of water transport capacity is lost due to cavitation. While loss of hydraulic conductance cannot be calculated using OVT data, a number of studies show strong agreement between vulnerability indices generated using the OVT and other accepted hydraulic techniques in leaves (Brodribb et al., 2016b; Skelton et al., 2018) and stems (Brodribb et al., 2017; Gauthey et al., 2020). This suggests that in these studies, stem cavitation events resolved using the OVT are representative of cavitation events in the rest of the stem, thus providing important information about vulnerability to drought and propagation of cavitation events, as well as impacts on water transport capacity of the whole stem. However, it must be noted that cavitation could only be reliably resolved to a shallow depth in these stems using the OVT, demonstrating a limitation of this technique that may have implications for detecting cavitation in larger stems and in stems with certain xylem arrangements.

The reliability of the OVT for recording cavitation to a depth of 0.3 mm indicates its suitability for current-year stems, but not necessarily for large stems with deep sapwood. However, given that cavitation in woody stems is irreparable in most species (Brodersen and McElrone 2013; Charrier et al., 2016; Choat et al., 2019), and most water transport occurs through current-year xylem (Ellmore and Ewers 1986; Melcher et al., 2003; Fukuda et al., 2015), the vulnerability of this superficial xylem is likely to reflect susceptibility of the whole plant to damage (Fukuda et al., 2015). Thus, observations of fully developed xylem proximate to the bark are highly relevant for studying the functional status of trees. It may also be possible to determine representative vulnerability to cavitation even from the surface of larger stems, but this remains to be tested.

In the third experimental species, *E. globulus*, the OVT detected ~33% more cavitations from the xylem surface to a depth of 0.3 mm into the stem compared to microCT. This variation could be attributed to the stem anatomy of our *E. globulus* sample and the resolution limits of microCT in this study. In the *E. globulus* stem, xylem vessels were arranged in two bands, with a band of large xylem vessels nearest to the surface and a band of smaller xylem vessels very close to the pith (Supplemental Fig. S5), in contrast to the other species, which had more uniform vessel arrangements (Supplemental Figs. S6 and S7). The higher resolution of the OVT compared with that of microCT means that the OVT had greater capacity to detect smaller cavitations, which likely occurred in the smaller, deeper conduits. These smaller conduits may include vasicentric tracheids, which are present in *E. globulus* (Wheeler, 2011). The microCT scans had a pixel size of 8.7 μm in this study, meaning that ~4 pixels were required to reliably resolve an individual xylem vessel. This meant that only vessels >34.8 μm in diameter were included in the microCT cavitation counts. However, a large proportion (57%) of vessels within the region visualized using the OVT from the xylem surface to a depth of 0.3 mm were <35 μm in diameter. These vessels were not resolved using microCT. In contrast, the OVT had a pixel size of 3.6 μm, and in *E. globulus*, nearly all xylem vessels were located from the xylem surface to a depth of 0.3 mm, making it likely that cavitation in these smaller conduits was detectable in the OVT images but not easily detectable in the microCT scans.

CONCLUSIONS

Here we use a new dynamic method to reveal that >80% of xylem cavitation events in the stems of our three long-vesseled angiosperm species were discrete, single-vessel events. This contrasts with previous research in leaves suggesting that cavitation propagates largely by multiple events. As the leaf vein network is much more highly interconnected than the xylem network in stems, and increased connectivity is thought to lead to a higher probability of vessel-vessel cavitation spread, this suggests that there is a strong link between vessel connectivity and the pattern of embolism spread. The higher degree of vessel grouping and higher frequency of multiple cavitation events found in *A. mearnsii* compared to *A. verticillata* and *E. globulus* indicates that differences in the degree of xylem network connectivity may also explain differences in the frequency of single versus multiple cavitation events between the same organ in different species. Application of optical imaging of cavitation across additional species with a diverse range of xylem anatomies will allow us to determine the relationship between embolism spread and xylem network arrangement.

MATERIALS AND METHODS

Plant Material

Branches ~1 m in length were collected from three cavitation-resistant species near the University of Tasmania's Sandy Bay campus (Hobart, Tasmania, Australia). Branches were collected early in the morning (~8:00 AM) during spring, when levels of cavitation were minimal. Samples were collected from a single adult tree of *Acacia mearnsii*, *Allocasuarina verticillata*, and *Eucalyptus globulus* which with stem P50s between −5 and −8 MPa (Brodribb et al., 2016a; Smith-Martin et al., 2020). Branches were carefully sealed within two thick plastic bags containing damp paper towel to prevent water loss. Branches were then transported from Tasmania to the Australian Synchrotron in Melbourne, where initial scans were made ~24 h after branch collection.

Sample Site Preparation

OVT devices (details provided below) were mounted to stems in a way that allowed simultaneous imaging of the same region of stem with both the OVT and microCT. Before imaging commenced, branches were removed from the bags and a small area of bark (~1 cm^2) was removed from one side of the stem ~10 to 20 cm from the tip of the branch (~80 cm from the cut end) to view the xylem. We found that the amount of cavitation induced by careful bark removal and application of a thin layer of adhesive hydrogel (Tensive Conductive Adhesive Gel, Parker Laboratories) was negligible using a single branch of *A. mearnsii* (Fig. 7; Supplemental Fig. S2).

We used a modified version of the methods described by Brodribb et al. (2016a) to capture the temporal and spatial pattern of embolism spread in current-year xylem for one branch of each of the three species. Young stem segments ~2 to 3 mm in diameter were used, restricting observations to the present-year xylem. An adhesive hydrogel (Tensive) was applied to the exposed xylem to improve light transmission and reduce evaporative water loss. A custom-built camera, MiCAM (timelapse camera for the raspberry pi; https://micams.co.), was then attached to this region and images of the stem were captured every 2 min (see http://www.opensourceov.org/ for detailed instructions related to construction, use, and data analysis). These images recorded changes to the intensity of light reflected from the xylem, which are associated with cavitation events as the branches dried (Brodribb et al., 2016a). A stem psychrometer (PSY, ICT International) was attached to each branch, either to a side branch or to the main axis, 50 cm from the MiCAM (~50 cm from the cut end) to monitor water potential. Water potential readings were taken at 10-min intervals, and a Scholander pressure chamber was used to periodically cross-validate these measurements using leaves. Images captured using the MiCAM were monitored for cavitation. Cavitation events were identified using image subtraction (see "Quantifying Cavitation") following the methods in Brodribb et al. (2016a).

Upon observation of more than three cavitation events in OVT images, sample sites were scanned in the medical imaging beamline (IMBL) at the Australian Synchrotron. The top half of the MiCAM (which contains the camera) was removed from the branch before scanning to prevent damage to the camera electronics, while the base was left secured to the branch. The base of the clamp provided a guide to align the sample for microCT scans (the crosshairs of the beamline were lined up with the middle of the area of exposed xylem in the IMBL hutch) and ensured that the location of the OVT scan area remained unchanged when the top part of the MiCAM was then reattached after the microCT scan. After initial setup, a robotic arm (KR1000 Titan, Kuka) positioned the sample in the beamline. Scans were made at an x-ray energy of 30 keV, while the sample was rotated through 180° with scans taken at 0.1 angle increments (scan field of view 28 × 20 mm). This produced 1,800 scans with additional flat-field and dark-field images recorded before and after each scan. Total scan time was 18 to 23 min, with exposure at each angle lasting 0.45 to 0.60 s. Scan volumes were reconstructed using XLICT Workflow 2015 (CSIRO) with the Gridrec reconstruction algorithm. Scanned image resolution was 8.7 μm^3 per voxel.

After initial scans, branches were removed from the hutch, the MiCAM was reattached, and branches were allowed to dry for ~4 h or until more than three events were observed in the OVT images. At this point, the microCT scan was repeated as above. This procedure was repeated three to four times, until leaf desiccation was observed in samples. Finally, stems were cut 3 cm from the scan point to ensure that all vessels were air filled, and a final scan was made to count the total number of vessels. Samples were then sectioned through the scan site, mounted on a slide, and photographed with a Leica DM 1000 microscope with a 1× tube and a 4× objective (magnification) and resolution of 2,560 × 1,920 pixels.

Matching Cavitated Xylem Vessels

Three-dimensional renderings of the stem region scanned using microCT were created with Drishti, version 2.6.2 (Limaye 2012). From the 1,800 scanned images, ~500 microCT images from within the area visualized using the OVT were selected to construct 3D renderings. The OVT-visualized area was identified by locating the range of microCT images showing the region of the stem where bark had been removed for the OVT. After 3D reconstruction using Drishti, surface features in both the 3D rendering and the OVT images were used to orientate the 3D rendering into the same position as in the OVT images. Avizo 2019 software (Thermo Fisher Scientific) was then used to visualize and highlight the vessels of interest that appeared embolized in both the microCT and OVT images. This allowed us to identify the same cavitated vessels in both the OVT images and the 3D renderings.

Quantifying Cavitation

MicroCT

Single transverse images from microCT scans were used to count the number of cavitated vessels in each of the scans. Images were selected using visual reference points to provide good correspondence between microCT images and the region of interest captured by the OVT using MiCAMs. In each species, the stem pith was ~0.6 mm from the peeled surface. Because it is unlikely that cavitated vessels can be observed beyond the pith using the OVT, 0.6 mm was assumed to be the maximum depth at which vessels could be observed. Thus, the number of cavitated vessels in the stem tissue from the xylem surface to depths of 0.3 and 0.6 mm into the stem were counted within the whole stem area from transverse microCT images (Fig. 8). These depths were measured from the middle of the area where xylem was exposed, as this central point was thought to represent an average of the possible orientations of the stem in the OVT images (Fig. 8). Cavitated vessels were clearly distinguishable because of the difference in voxel intensity in air-filled versus water-filled vessels.

The total number of vessels counted from microCT images was expressed as a percentage of the total vessels, which was obtained from scans of cut branches. Total vessel counts from cut scans were validated against transverse sections of the stems using light microscopy (Supplemental Fig. S8). Light microscope images were then processed in ImageJ to isolate vessels as ellipses. Vessels were sorted into diameter-size classes scaled by the pixel size in the microCT images (1–10 pixels, where 1 pixel = 8.7 μm) and the number of vessels was counted at each of these pixel-size thresholds. Only vessels that were >4 pixels (34.8 μm) in diameter could be confidently resolved in microCT images, so vessel counts from light microscope images were filtered to include only vessels >34.8 μm in diameter. In *A. verticillata* and *E. globulus*, approximately half of stem vessels were below this size threshold (66% and 57%, respectively), while in *A. mearnsii* only 25% were below the threshold. Counts of the vessels with a diameter >34.8 μm from the microCT scans corresponded with vessel counts from microscope sections (Supplemental Fig. S8). The cumulative number of vessels that cavitated between one microCT scan and the next was then compared to the cumulative number of new vessels observed using the OVT to determine how closely the vessel counts matched between the two techniques.

OVT

Changes in light reflection due to cavitation between sequential images collected using the OVT were identified using ImageJ by subtracting images from each other in sequence. The pixel area of cavitation events was measured by highlighting groups of aggregated pixels over a certain size threshold using the "threshold" tool in the IMAGEJ "analyze" menu (Brodribb et al., 2016a). Image noise not associated with cavitation events (i.e. due to slower movement during desiccation) was then removed to produce a stack of images containing only cavitation events (see http://www.opensourceov.org/ for full details). A 4-mm-long section was cropped from the middle of the 8-mm-long OVT scans and was used to count the number of cavitations (Fig. 9). This middle section of the OVT scans has the highest image quality due to the focus of the MiCAM images. MicroCT scans were aligned with the middle of the xylem area visualized using the OVT to ensure that the vessels counted in the OVT images were also captured in the microCT scans (Fig. 9). Three narrow sections (10 pixels wide) were taken from the right, middle, and left of the 4-mm sections of OVT images orientated so that vessels were horizontal, and the number of vessels observed in each section was counted. The average of these three counts was used in the analysis, as this was deemed most likely to represent the cavitations

that would be present in the single microCT scan used to count the cavitated vessels.

The number of spatially separated cavitation events was counted for each OVT image in the three narrow sections taken from the 4-mm-long substack of the OVT image stack (described in the previous paragraph), and an average count of multiple events across these three stacks was used. The frequency of single events (one cavitated vessel in a single plane in an image) and multiple events (more than one spatially distinct cavitation in a single image, representing 2 min) per image was compared. The largest cavitation events in all species comprised >4% of the total pixel area of cavitated vessels. Within stems these large events together accounted for ~30% to 60% of the total pixel area of cavitated vessels (see Fig. 4). Thus, we divided events into larger (>4% of total pixel area of cavitated vessels) and smaller events for analysis.

Vessel Characteristics

Vessel Size Distribution

Vessel diameters of the three experimental species were measured from light microscope images of transverse sections through the stem region where cavitation events were observed using microCT and the OVT (one stem per species). Vessels were measured within a region from the xylem surface to a depth of 0.3 mm into the stem, as described above. ImageJ was used to isolate vessels as ellipses and calculate vessel diameters. These diameters were then expressed as vessel size distributions using histograms in Sigmaplot version 12.5 (Systat Software).

Vessel Grouping

A vessel grouping index (V_G) was calculated for each species using light microscope images according to the methods of Carlquist (2001) and Scholz et al. (2013). The V_G describes how vessels are connected in the transverse plane. The total number of vessels was counted within the OVT-visualized region from the xylem surface to a depth of 0.3 mm into the stem. This was divided by the total number of vessel groupings in this region (the number of solitary vessels plus the number of vessels in groups). A V_G index of 1 indicates that all vessels are solitary, and an index >1 indicates increasing degrees of vessel grouping.

Statistical Analysis

Data were plotted using Sigmaplot version 12.5 (Systat Software). Drishti verson 2.6.2 (Limaye, 2012), and Avizo software (Thermo Fisher Scientific) were used to create 3D renderings of microCT scans to visualize vessel networks within stems.

Supplemental Data

The following supplemental materials are available.

Supplemental Figure S1. Scans of each of the three stems showing the peeled stem with tensive hydrogel.

Supplemental Figure S2. Relationship between cavitated vessels detected from the xylem surface to a depth of 0.3 mm under a region of stem with the bark removed.

Supplemental Figure S3. Vessel size distributions for the stems of each of the three species, *A. mearnsii*, *A. verticillate*, and *E. globulus*.

Supplemental Figure S4. A raw image of half of a *Eucryhpia moorei* leaf and a multivein cavitation event in the same leaf.

Supplemental Figure S5. A transverse light microscope section of the OVT-visualized region in the *E. globulus* stem.

Supplemental Figure S6. A transverse light microscope section of a representative *Acacia mearnsii* stem showing the vessel arrangement.

Supplemental Figure S7. A transverse light microscope section of a representative *A. verticillata* stem showing the vessel arrangement.

Supplemental Figure S8. Numbers of vessels counted from light microscope transverse sections.

ACKNOWLEDGMENTS

We thank Alice Gauthey and Jennifer Peters for assistance during the experiments at the IMBL.

Received April 16, 2020; accepted June 15, 2020; published June 24, 2020.

LITERATURE CITED

Allen CD, Breshears DD, McDowell NG (2015) On underestimation of global vulnerability to tree mortality and forest die-off from hotter drought in the Anthropocene. Ecosphere **6:** 1–55

Anderegg WRL, Klein T, Bartlett M, Sack L, Pellegrini AF, Choat B, Jansen S (2016) Meta-analysis reveals that hydraulic traits explain cross-species patterns of drought-induced tree mortality across the globe. Proc Natl Acad Sci USA **113:** 5024–5029

Brodersen CR, McElrone AJ (2013) Maintenance of xylem network transport capacity: A review of embolism repair in vascular plants. Front Plant Sci **4:** 108

Brodersen CR, McElrone AJ, Choat B, Lee EF, Shackel KA, Matthews MA (2013) In vivo visualizations of drought-induced embolism spread in *Vitis vinifera*. Plant Physiol **161:** 1820–1829

Brodribb TJ, Bienaimé D, Marmottant P (2016a) Revealing catastrophic failure of leaf networks under stress. Proc Natl Acad Sci USA **113:** 4865–4869

Brodribb TJ, Carriqui M, Delzon S, Lucani C (2017) Optical measurement of stem xylem vulnerability. Plant Physiol **174:** 2054–2061

Brodribb TJ, Cochard H (2009) Hydraulic failure defines the recovery and point of death in water-stressed conifers. Plant Physiol **149:** 575–584

Brodribb TJ, Powers J, Cochard H, Choat B (2020) Hanging by a thread? Forests and Drought. Science **368:** 261–266

Brodribb TJ, Skelton RP, McAdam SA, Bienaimé D, Lucani CJ, Marmottant P (2016b) Visual quantification of embolism reveals leaf vulnerability to hydraulic failure. New Phytol **209:** 1403–1409

Carlquist S (1966) Wood anatomy of Compositae: A summary, with comments on factors controlling wood evolution. Aliso **6:** 25–44

Carlquist S (1984) Vessel grouping in dicotyledon wood. Aliso **10:** 505–525

Carlquist S (1986) Terminology of imperforate tracheary elements: A reply. IAWA J **7:** 168–170

Carlquist S (2001) Comparative Wood Anatomy—Systematic, Ecological, and Evolutionary Aspects of Dicotyledon Wood, 2nd ed. Springer, Berlin

Charrier G, Torres-Ruiz JM, Badel E, Burlett R, Choat B, Cochard H, Delmas CE, Domec JC, Jansen S, King A, et al (2016) Evidence for hydraulic vulnerability segmentation and lack of xylem refilling under tension. Plant Physiol **172:** 1657–1668

Chatelet DS, Matthews MA, Rost TL (2006) Xylem structure and connectivity in grapevine (*Vitis vinifera*) shoots provides a passive mechanism for the spread of bacteria in grape plants. Ann Bot **98:** 483–494

Choat B, Badel E, Burlett R, Delzon S, Cochard H, Jansen S (2016) Non-invasive measurement of vulnerability to drought-induced embolism by x-ray microtomography. Plant Physiol **170:** 273–282

Choat B, Brodersen CR, McElrone AJ (2015) Synchrotron x-ray microtomography of xylem embolism in *Sequoia sempervirens* saplings during cycles of drought and recovery. New Phytol **205:** 1095–1105

Choat B, Cobb AR, Jansen S (2008) Structure and function of bordered pits: New discoveries and impacts on whole-plant hydraulic function. New Phytol **177:** 608–625

Choat B, Jansen S, Brodribb TJ, Cochard H, Delzon S, Bhaskar R, Bucci SJ, Feild TS, Gleason SM, Hacke UG, et al (2012) Global convergence in the vulnerability of forests to drought. Nature **491:** 752–755

Choat B, Nolf M, Lopez R, Peters JMR, Carins-Murphy MR, Creek D, Brodribb TJ (2019) Non-invasive imaging shows no evidence of embolism repair after drought in tree species of two genera. Tree Physiol **39:** 113–121

Christman MA, Sperry JS, Smith DD (2012) Rare pits, large vessels and extreme vulnerability to cavitation in a ring-porous tree species. New Phytol **193:** 713–720

Cochard H, Delzon S, Badel E (2015) X-ray microtomography (micro-CT): A reference technology for high-resolution quantification of xylem embolism in trees. Plant Cell Environ **38:** 201–206

Dixon HH (1914) Transpiration and the Ascent of Sap in Plants. Macmillan, London

Dixon HH, Joly J (1895) On the ascent of sap. Philos Trans R Soc Lond B Biol Sci **186:** 563–576

Ellmore GS, Ewers FW (1986) Fluid flow in the outermost xylem increment of a ring-porous tree, *Ulmus americana*. Am J Bot **73:** 1771–1774

Fukuda K, Kawaguchi D, Aihara T, Ogasa MY, Miki NH, Haishi T, Umebayashi T (2015) Vulnerability to cavitation differs between current-year and older xylem: Non-destructive observation with a compact magnetic resonance imaging system of two deciduous diffuse-porous species. Plant Cell Environ **38:** 2508–2518

Gauthey A, Peters JMR, Carins-Murphy MR, Rodriguez-Dominguez CM, Li X, Delzon S, King A, Medlyn BE, Tissue DT, Brodribb TJ, et al (2020) Evaluating methods used to measure cavitation resistance in seven woody species with differing xylem anatomy: A comparison of visual and hydraulic techniques. New Phytol doi:10.1111/nph.16746

Hacke UG, Sperry JS (2001) Functional and ecological xylem anatomy. Perspect Plant Ecol Syst **4:** 97–115

Johnson KM, Jordan GJ, Brodribb TJ (2018) Wheat leaves embolized by water stress do not recover function upon rewatering. Plant Cell Environ **41:** 2704–2714

Knipfer T, Brodersen CR, Zedan A, Kluepfel DA, McElrone AJ (2015) Patterns of drought-induced embolism formation and spread in living walnut saplings visualized using x-ray microtomography. Tree Physiol **35:** 744–755

Larter M, Pfautsch S, Domec JC, Trueba S, Nagalingum N, Delzon S (2017) Aridity drove the evolution of extreme embolism resistance and the radiation of conifer genus *Callitris*. New Phytol **215:** 97–112

Lee EF, Matthews MA, McElrone AJ, Phillips RJ, Shackel KA, Brodersen CR (2013) Analysis of HRCT-derived xylem network reveals reverse flow in some vessels. J Theor Biol **333:** 146–155

Lewis AM (1988) A test of the air-seeding hypothesis using *sphagnum* hyalocysts. Plant Physiol **87:** 577–582

Limaye A (2012) Drishti: A volume exploration and presentation tool. Proc SPIE 8506, Developments in X-Ray Tomography **VIII:** 85060X

Loepfe L, Martinez-Vilalta J, Piñol J, Mencuccini M (2007) The relevance of xylem network structure for plant hydraulic efficiency and safety. J Theor Biol **247:** 788–803

Maherali H, Pockman WT, Jackson RB (2004) Adaptive variation in the vulnerability of woody plants to xylem cavitation. Ecology **85:** 2184–2199

Medeiros JS, Lens F, Maherali H, Jansen S (2019) Vestured pits and scalariform perforation plate morphology modify the relationships between angiosperm vessel diameter, climate and maximum plant height. New Phytol **221:** 1802–1813

Melcher PJ, Zwieniecki MA, Holbrook NM (2003) Vulnerability of xylem vessels to cavitation in sugar maple. Scaling from individual vessels to whole branches. Plant Physiol **131:** 1775–1780

Millar CI, Stephenson NL (2015) Temperate forest health in an era of emerging megadisturbance. Science **349:** 823–826

Mrad A, Domec JC, Huang CW, Lens F, Katul G (2018) A network model links wood anatomy to xylem tissue hydraulic behaviour and vulnerability to cavitation. Plant Cell Environ **41:** 2718–2730

Pittermann J, Stuart SA, Dawson TE, Moreau A (2012) Cenozoic climate change shaped the evolutionary ecophysiology of the Cupressaceae conifers. Proc Natl Acad Sci USA **109:** 9647–9652

Schenk HJ, Espino S, Goedhart CM, Nordenstahl M, Cabrera HI, Jones CS (2008) Hydraulic integration and shrub growth form linked across continental aridity gradients. Proc Natl Acad Sci USA **105:** 11248–11253

Scholz A, Klepsch M, Karimi Z, Jansen S (2013) How to quantify conduits in wood? Front Plant Sci **4:** 56

Sheil D (2014) How plants water our planet: Advances and imperatives. Trends Plant Sci **19:** 209–211

Skelton RP, Dawson TE, Thompson SE, Shen Y, Weitz AP, Ackerly D (2018) Low vulnerability to xylem embolism in leaves and stems of North American oaks. Plant Physiol **177:** 1066–1077

Skelton RP, West AG, Dawson TE (2015) Predicting plant vulnerability to drought in biodiverse regions using functional traits. Proc Natl Acad Sci USA **112:** 5744–5749

Smith-Martin CM, Skelton RP, Johnson KM, Lucani C, Brodribb TJ (2020) Lack of vulnerability segmentation among woody species in a diverse dry sclerophyll woodland community. Funct Ecol **34:** 777–787

Sperry JS, Saliendra NZ, Pockman WT, Cochard H, Cruizait P, Davis SD, Ewers FW, Tyree MT (1996) New evidence for large negative xylem pressures and their measurement by the pressure chamber method. Plant Cell Environ **19:** 427–436

Tyree MT, Sperry JS (1988) Do woody plants operate near the point of catastrophic xylem dysfunction caused by dynamic water stress?: Answers from a model. Plant Physiol **88:** 574–580

Tyree MT, Zimmermann MH (2002) Hydraulic Architecture of Whole Plants and Plant Performance. In MT Tyree, and MH Zimmermann, eds, Xylem Structure and the Ascent of Sap. Springer, Berlin-Heidelberg, pp 175–214

Venturas MD, Pratt RB, Jacobsen AL, Castro V, Fickle JC, Hacke UG (2019) Direct comparison of four methods to construct xylem vulnerability curves: Differences among techniques are linked to vessel network characteristics. Plant Cell Environ **42:** 2422–2436

Venturas MD, Rodriguez-Zaccaro FD, Percolla MI, Crous CJ, Jacobsen AL, Pratt RB (2016) Single vessel air injection estimates of xylem resistance to cavitation are affected by vessel network characteristics and sample length. Tree Physiol **36:** 1247–1259

Wason JW, Anstreicher KS, Stephansky N, Huggett BA, Brodersen CR (2018) Hydraulic safety margins and air-seeding thresholds in roots, trunks, branches and petioles of four northern hardwood trees. New Phytol **219:** 77–88

Wheeler E (2011) Insidewood—A web resource for hardwood anatomy. IAWA J **32:** 199–211

Wheeler JK, et al (2005) Inter-vessel pitting and cavitation in woody Rosaceae and other vesselled plants: A basis for a safety versus efficiency trade-off in xylem transport. Plant Cell Environ **28:** 800–812

Young DJ, Stevens JT, Earles JM, Moore J, Ellis A, Jirka AL, Latimer AM (2017) Long-term climate and competition explain forest mortality patterns under extreme drought. Ecol Lett **20:** 78–86

Zhao X (2016) Spatial variation of vessel grouping in the xylem of *Betula platyphylla* Roth. J Plant Res **129:** 29–37